



# Selective conversion of 5-hydroxymethylfurfural to diketone derivatives over Beta zeolite-supported Pd catalysts in water

Rubén Ramos<sup>a</sup>, Alexios Grigoropoulos<sup>a</sup>, Ben L. Griffiths<sup>a,b</sup>, Alexandros P. Katsoulidis<sup>a</sup>, Marco Zanella<sup>a</sup>, Troy D. Manning<sup>a</sup>, Frédéric Blanc<sup>b,c</sup>, John B. Claridge<sup>b</sup>, Matthew J. Rosseinsky<sup>a,\*</sup>

<sup>a</sup> Materials Innovation Factory, University of Liverpool, Liverpool L7 3NY, UK

<sup>b</sup> Department of Chemistry, University of Liverpool, Liverpool L69 7ZD, UK

<sup>c</sup> Stephenson Institute for Renewable Energy, University of Liverpool, Liverpool L69 7ZF, UK

## ARTICLE INFO

### Article history:

Received 6 December 2018

Revised 30 March 2019

Accepted 23 April 2019

### Keywords:

5-Hydroxymethylfurfural

HMF conversion

Beta zeolite

Supported Pd catalyst

Hydrogenation

Furan ring-opening

## ABSTRACT

Conversion of 5-hydroxymethylfurfural (HMF) in water to the linear diketone derivatives 1-hydroxyhexane-2,5-dione (HHD) and 2,5-hexanedione (HXD) was investigated over a series of Beta zeolite-supported transition metal catalysts (Co, Ni, Cu, Ru, Pd). Their catalytic performance was tested in a batch stirred reactor ( $T = 110\text{ }^{\circ}\text{C}$ ,  $P_{\text{H}_2} = 20\text{ bar}$ ) with Pd showing the highest activity and selectivity to HHD and HXD. The effects of Pd particle size, zeolite Si/Al ratio and reaction conditions ( $T = 80\text{--}155\text{ }^{\circ}\text{C}$ ,  $P_{\text{H}_2} = 5\text{--}60\text{ bar}$ ) were also investigated. The incorporation of Pd into Beta zeolite by the deposition-coprecipitation method produced the most efficient catalyst, affording complete HMF conversion ( $T = 110\text{ }^{\circ}\text{C}$ ,  $P_{\text{H}_2} = 60\text{ bar}$ ) predominantly to HHD (68% selectivity) and HXD (8% selectivity). The combination of a bifunctional acid/redox solid catalyst and water enhances the hydrolytic ring-opening and subsequent hydrogenation of the furan ring. Catalytic activity can be partially restored by a simple regeneration treatment. This work establishes a catalytic route to produce valuable diketone derivatives from renewable furanic platform sources in water.

© 2019 Elsevier Inc. All rights reserved.

## 1. Introduction

Non-edible lignocellulose is the most abundant, cheapest and fastest growing sustainable biomass resource, composed of three primary biopolymers: cellulose (a polymer of glucose), hemicellulose (a polymer mainly of pentoses) and lignin (a highly cross-linked polymer of substituted phenols) [1]. In order to produce value-added bio-products which could displace petroleum feedstocks, lignocellulose must first be transformed into simpler and more easily processed platform chemicals. This approach, similar to that used in conventional petroleum refineries, would allow the simultaneous production of biofuels and biochemicals in an integrated facility, a biorefinery [2].

**Abbreviations:** HMF, 5-hydroxymethylfurfural; HHD, 1-hydroxyhexane-2,5-dione; HXD, 2,5-hexanedione; FDM, furan-2,5-diylidimethanol; THFDM, tetrahydrofuran-2,5-diylidimethanol; DMF, 2,5-dimethylfuran; HCPN, 3-hydroxymethylcyclopentanone; HCPL, 3-hydroxymethylcyclopentanol; HHED, 1-hydroxyhex-3-ene-2,5-dione.

\* Corresponding author at: Department of Chemistry, Materials Innovation Factory, University of Liverpool, Liverpool L7 3NY, UK.

E-mail address: [m.j.rosseinsky@liverpool.ac.uk](mailto:m.j.rosseinsky@liverpool.ac.uk) (M.J. Rosseinsky).

<https://doi.org/10.1016/j.jcat.2019.04.038>

0021-9517/© 2019 Elsevier Inc. All rights reserved.

In 2004, the U.S. Department of Energy (DOE) [3] released a report, later revised by Bozell *et al.* [4], identifying the top value-added platform chemicals in a future biorefinery. HMF was identified as one of the most appealing and promising building block molecules. This furan derivative can be produced from agricultural waste and forest residue such as polysaccharides (*i.e.* cellulose and hemicellulose) by acid-catalysed hydrolysis to C<sub>6</sub> monosaccharides, followed by dehydration [5]. In contrast to most petrochemical products, HMF is an oxygen-rich, functionalized compound. Its conversion to value-added chemicals usually involves several chemical transformations (*e.g.* hydrogenation, dehydration, hydrogenolysis, oxidation, *etc.*) which are promoted by multifunctional heterogeneous catalysts [6,7]. The development of related catalytic heterogeneous processes has become highly topical to produce valuable bioproducts such as: tetrahydrofuran 2,5-diylidimethanol (THFDM) [8–10], 2,5-dimethylfuran (DMF) [11], 2,5-furandicarboxylic acid (FDCA) [12,13], C<sub>6</sub> linear alcohols [14,15], 3-hydroxymethylcyclopentanone (HCPN) and 3-hydroxymethylcyclopentanol (HCPL) [16,17] (Fig. 1).

One much less studied reaction is the conversion of HMF into the linear diketone derivatives 1-hydroxyhexane-2,5-dione

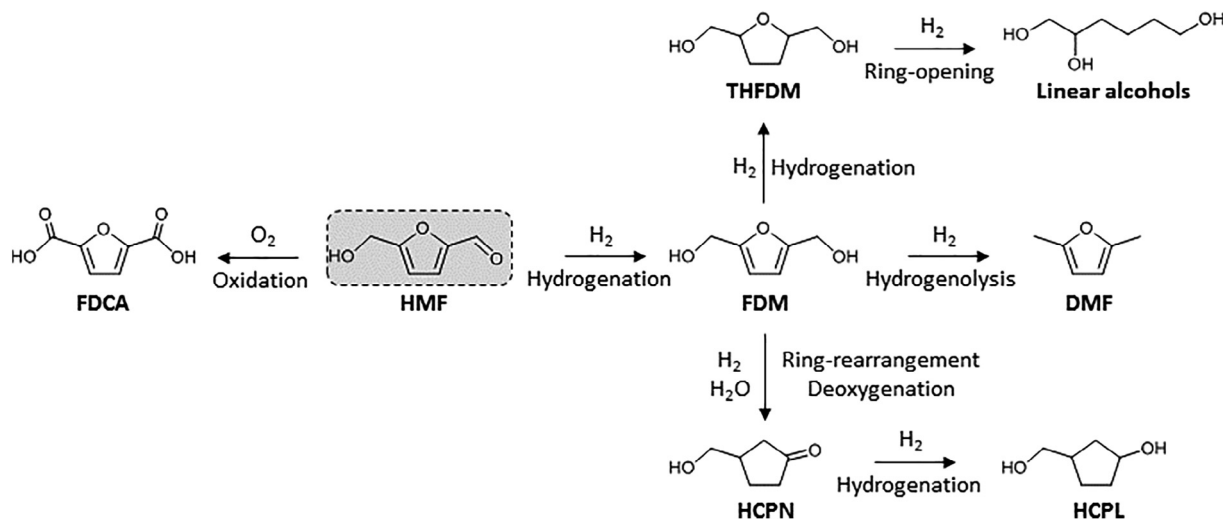


Fig. 1. Chemical transformation of HMF into various biomass-derived compounds [8–17].

(HHD) and 2,5-hexanedione (HXD). Although a large-scale synthetic route to HHD is currently not available, the presence of a hydroxymethyl functionality offers opportunities for the synthesis of valuable chemicals, as recently highlighted [18–20]. HXD is employed as a solvent and as an intermediate for the synthesis of polymers, amines and surfactants [21,22]. HHD can be produced from HMF in water under  $H_2$  pressure via the metal-catalysed selective hydrogenation of the carbonyl group to furan-2,5-diylidimethanol (FDM), followed by the acid-catalysed ring-opening of the FDM unsaturated ring [23]. Notably, this pathway does not involve the formation of a more stable saturated tetrahydrofuran ring, whose ring-opening requires harsh reaction conditions (*i.e.*  $T > 140\text{ }^\circ\text{C}$ ;  $P > 60\text{ bar}$ ) [24]. HXD can also be produced from FDM via hydrogenolysis to DMF, followed by hydrolytic ring-opening of the latter or by HHD via scission of the hydroxyl group (Fig. 2) [22,25].

The formation of HHD from HMF was firstly reported in 1991 by Schiavo *et al.* using Pd/C in an aqueous solution of oxalic acid ( $\text{pH} = 2$ ) at 70 bar  $H_2$  and  $140\text{ }^\circ\text{C}$  [23]. In 2009, Luijckx *et al.* reported a similar process using HCl [26]. In 2014, Liu *et al.* developed two binary catalytic systems using Pd/C either in  $\text{CO}_2/\text{H}_2\text{O}$  (forming carbonic acid) [27], or in THF with co-added Amberlyst-15 [28], affording in both cases 77% yield of HHD (see Table S11). Recently we reported that HHD is formed as a low yield intermediate ( $<7\%$ ) in the conversion of HMF to HCPN and HCPL over  $\text{M-Al}_2\text{O}_3$  catalysts in  $\text{H}_2\text{O}$  ( $\text{M} = \text{Co}, \text{Ni}, \text{Cu}$ ). HHD was rapidly converted to HCPN via an aldol condensation reaction, catalysed by basic sites, followed by hydrogenation [17].

The requirement of hydrogenating metal phases and acidic sites for the production of HHD prompted us to investigate the deposition of various transition metals over zeolite supports to prepare

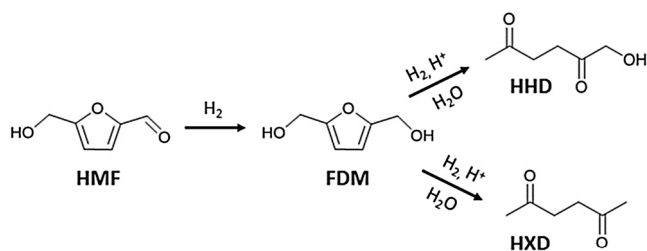


Fig. 2. Catalytic reaction pathway discussed in this work for the conversion of HMF to the linear diketone derivatives HHD and HXD via the acid-catalysed hydrolytic ring-opening of FDM.

easily tuneable bifunctional catalysts. Among the most investigated zeolites, Beta (with BEA topology) exhibits excellent properties to the aimed transformation due to its high hydrothermal stability, large specific surface area ( $>600\text{ m}^2\text{ g}^{-1}$ ), 3D large-pore channel system (5.5–7.6 Å) and dual Lewis/Brønsted acidity [29]. Beta zeolite-based catalysts have been used for the conversion of furfural into levulinic acid [30,31] and for the hydrodeoxygenation of furoins into alkanes [32]. However, to the best of our knowledge, there are no studies reporting the formation of linear diketone derivatives using Beta zeolite-supported catalysts.

Herein, we present the catalytic production of the diketone derivatives HHD and HXD from HMF by zeolite-supported transition metals in  $\text{H}_2\text{O}$ . A series of transition metal-loaded (M) Beta zeolites were prepared ( $\text{M} = \text{Co}, \text{Ni}, \text{Cu}, \text{Ru}, \text{Pd}$ ), characterised and tested in a batch stirred reactor under  $H_2$  pressure with Pd showing the highest catalytic activity. Consequently, the effects of Pd particle size, zeolite Si/Al ratio and reaction conditions were investigated, and catalyst stability and recyclability were evaluated. This work establishes Beta zeolite-supported Pd catalysts as promising candidates for the upgrading of HMF into valuable biomass-derived linear diketone derivatives by demonstrating for the first time the conversion of HMF to HHD and HXD in water by a solid state, bifunctional (no acid co-added) catalyst.

## 2. Experimental

### 2.1. Catalyst preparation

Metal-loaded zeolites were prepared by incipient wetness impregnation (IWI) of commercially available Beta (Si/Al = 12.5) and ZSM-5 (Si/Al = 11.5) zeolites purchased from Zeolyst Int. The corresponding aqueous solutions of the metal precursors were prepared using:  $\text{PdCl}_2$  (Sigma-Aldrich),  $\text{Pd}(\text{NO}_3)_2 \cdot 2\text{H}_2\text{O}$  (Aldrich),  $\text{RuCl}_3$  (Aldrich),  $\text{NiCl}_2 \cdot 6\text{H}_2\text{O}$  (Aldrich),  $\text{CuCl}_2 \cdot 2\text{H}_2\text{O}$  (Aldrich) and  $\text{CoCl}_2 \cdot 6\text{H}_2\text{O}$  (Fluka). Prior to impregnation, the parent  $\text{NH}_4$ -zeolites were calcined at  $550\text{ }^\circ\text{C}$  (heating rate of  $2\text{ }^\circ\text{C min}^{-1}$ ) in static air for 5 h, producing the respective H-zeolites. The deposition of the metal was carried out by adding dropwise the aqueous solution of the precursor to the zeolite support at room temperature (3 wt% for the Pd and Ru samples; 10 wt% for the Cu, Ni and Co samples). After impregnation, the catalysts were dried in a rotary evaporator at  $65\text{ }^\circ\text{C}$  under vacuum for 1 h. Subsequently, the dried samples were calcined in air at  $500\text{ }^\circ\text{C}$  for 5 h (heating rate of  $2\text{ }^\circ\text{C min}^{-1}$ ). The reduction treatment was performed under

pure H<sub>2</sub> flow (100 cm<sup>3</sup> min<sup>-1</sup>) for 5 h at 200 °C (for the Pd and Ru samples), 300 °C (Cu sample) and 500 °C (Ni and Co samples) with a heating rate of 2 °C min<sup>-1</sup>. Finally, the catalysts were passivated under a flow of 1% v/v O<sub>2</sub>/N<sub>2</sub> (100 cm<sup>3</sup> min<sup>-1</sup>) for 2 h at room temperature.

Pd-loaded Beta zeolite was also prepared by deposition-coprecipitation (DP-CP) using the urea-based method developed by Geus *et al.* [33]. First, 2 g of the calcined Beta zeolite were placed in a 250 ml round-bottom flask. Then, an aqueous solution (100 ml) containing PdCl<sub>2</sub> (0.005 M) and urea (1.2 M, Sigma) was added dropwise with constant stirring (550 rpm) at room temperature. The suspension (pH = 4–4.5) was heated to 95 °C to initiate urea hydrolysis. After 3 h, the pH of the suspension remained stable at pH ≈ 7.5. The solution was cooled to room temperature and the precipitate was collected by filtration, washed with deionized water, dried at 110 °C overnight and subsequently calcined in air at 500 °C for 5 h (heating rate of 2 °C min<sup>-1</sup>). The calcined sample (catalyst precursor) was then reduced under pure H<sub>2</sub> flow (100 cm<sup>3</sup> min<sup>-1</sup>) at 200 °C for 5 h (heating rate of 2 °C min<sup>-1</sup>). Finally, the reduced catalyst was passivated under a flow of 1% v/v O<sub>2</sub>/N<sub>2</sub> (100 cm<sup>3</sup> min<sup>-1</sup>) for 2 h at room temperature. Hereafter, the sample prepared by the DP-CP urea method will be referred as Pd(u)/Beta.

Partial dealumination of the calcined Beta zeolite (Si/Al = 12.5) was carried out by acid treatment using HNO<sub>3</sub> aqueous solutions of different concentration (0.1, 0.5, 2 and 5 M) at room temperature for 1 h (20 mL g<sup>-1</sup> zeolite). After filtration and washing with deionized water, the materials were dried overnight (110 °C) and calcined in static air at 500 °C for 5 h (heating rate of 2 °C min<sup>-1</sup>). Afterwards, the obtained dealuminated zeolites were impregnated with Pd following the DP-CP urea method described above. Hereafter, the four dealuminated and impregnated samples will be abbreviated as Pd(u)/Beta-dAl<sub>x</sub> (x = 1–4), where x = 4 refers to the sample showing the highest degree of dealumination (higher Si/Al ratio).

## 2.2. Catalyst characterization

The prepared catalysts were characterised by powder X-Ray diffraction (PXRD) on a Panalytical X'Pert Pro diffractometer with Co K<sub>α1</sub> radiation (λ = 1.7890 Å) in the 2θ angle range 10–80° (scanning speed of 0.023° s<sup>-1</sup>). Metal content of the catalysts was determined by inductively coupled plasma - optical emission spectroscopy (ICP-OES) using an Agilent 5110 SVDV instrument. The samples were digested in a strong acidic medium (10 ml HCl and 20 ml HNO<sub>3</sub>) and then diluted with water (1:10 v/v). Textural properties were evaluated through N<sub>2</sub> adsorption-desorption isotherms at 77 K, using a Micromeritics TRISTAR II instrument. Prior to the measurement, the samples were outgassed under vacuum at 120 °C for 20 h. The BET equation was used for specific surface area calculation, whereas pore volume was determined by the BJH method.

Acidity of the catalysts was determined by temperature programmed desorption of ammonia (NH<sub>3</sub>-TPD) in a Quantachrome ChemBET 3000 unit. Firstly, the samples were outgassed under a He stream (100 cm<sup>3</sup> min<sup>-1</sup>) heating at 10 °C min<sup>-1</sup> up to 350 °C. Afterwards, the samples were cooled to 150 °C and saturated under an ammonia stream (100 cm<sup>3</sup> min<sup>-1</sup>) for 10 min. Subsequently, the physically adsorbed ammonia was removed by flowing helium (100 cm<sup>3</sup> min<sup>-1</sup>) for 30 min at 150 °C. Finally, the chemically adsorbed ammonia was desorbed by heating to 650 °C with a rate of 10 °C min<sup>-1</sup> under He flow (100 cm<sup>3</sup> min<sup>-1</sup>). Ammonia concentration was monitored continuously using a thermal conductivity detector (TCD).

Thermogravimetric analysis (TGA) was carried out on a Q600 TA Instrument; ca. 5 mg of sample were loaded into an alumina

microcrucible and heated to 800 °C at 10 °C min<sup>-1</sup> under a flow of air (100 cm<sup>3</sup> min<sup>-1</sup>). Elemental analysis (C and H content) of the used catalysts was carried out on a Thermo EA1112 Flash CHNS Analyser. TEM images were obtained with a JEOL 2100 transmission electron microscope operating at 200 kV. The samples were dispersed in acetone, stirred in an ultrasonic bath and deposited on a carbon-coated Cu grid. SEM imaging and energy-dispersive X-ray (EDX) spectroscopy were run on a Hitachi S-4800 Field-Emission scanning electron microscope.

Solid state <sup>27</sup>Al NMR experiments were performed on a 9.4 T Bruker DSX 400 MHz spectrometer using a Bruker Triple Resonance 4 mm HXY (in double resonance mode) probe under Magic Angle Spinning (MAS) at a rotational rate of 10 kHz. One-dimensional MAS NMR spectra were recorded using a rotor-synchronized (1 period) Hahn echo sequence with a radio frequency pulse of 50 kHz (π/2 pulse of 1.7 μs duration) and a quantitative recycle delay of 1 s. Whilst the quantitative interpretation of <sup>27</sup>Al MAS NMR data has to be performed with caution due to non-uniform excitation of sites with different magnitudes of the quadrupolar coupling constants [34], the similar values observed for tetrahedral and octahedral sites (*i.e.* 1–2 MHz) allow for an estimation of their ratio [35,36].

## 2.3. Catalytic experiments and product analysis

The performance of the catalysts was studied in high pressure 100 ml batch stirred reactors (Parr Instrument Co.) A glass liner was loaded with 45 ml of an aqueous solution of HMF (0.04 M) and 0.06 g of catalyst and placed into the stainless-steel reactor. After sealing the vessel, the reactor was flushed three times with N<sub>2</sub> and heated to the required reaction temperature (80–155 °C). Once the targeted temperature was reached, the vessel was pressurised with H<sub>2</sub> to the respective value (5–60 bar of H<sub>2</sub>) and stirring was set to 600 rpm. After the end of the reaction (typically 6 h), the identity and distribution of the products were determined by the combination of <sup>1</sup>H and <sup>13</sup>C NMR spectroscopy (Bruker AVANCE III HD spectrometer), GC-MS (Agilent 6890 N GC with a 5973 MSD detector) and GC (Agilent 7890A GC with an FID). GC and GC-MS were equipped with a DB-WAXetr capillary column (60 m, 0.25 mm i.d., 0.25 μm). Standard reference compounds used: HMF (Sigma), FDM (Manchester Organics), THFDM (Ambin-ter) and HXD (Sigma-Aldrich). Details regarding calculations of conversion, yield and selectivity are provided in the [Supporting Information](#) (SI).

## 3. Results and discussion

### 3.1. Active metal screening for the conversion of HMF into HHD and HXD

PXRD patterns (2θ = 10–80°) of the Beta-supported metal catalysts after reduction show the characteristic peaks of the corresponding metallic phase (Fig. S11). No crystalline phases of the metal oxides precursors were observed, confirming their complete reduction under the H<sub>2</sub> treatment. Well-defined reflections associated with the zeolitic structures (Beta or ZSM-5) were identified [37], verifying that crystallinity of the zeolitic support was preserved after impregnation. The composition of the prepared catalysts was determined by ICP-OES (Table 1), showing metal contents close to the corresponding nominal values (Pd, Ru = 2.7–2.9 wt%; Ni, Cu, Co = 8.7–9.3 wt%).

The comparison of the catalytic performance of several zeolite-supported metal catalysts, prepared by IWI, in the conversion of HMF is presented in Table 1 (110 °C, 20 bar H<sub>2</sub>). Temperature was set at 110 °C in order to minimize the extent of

**Table 1**Product distribution from the conversion of HMF over zeolite-supported metal catalysts prepared by incipient wetness impregnation.<sup>(a)</sup>

Entry	Catalyst	M <sup>(b)</sup> (wt%)	Conv. (%)	Selectivity (%)					C <sub>mb</sub> <sup>(c)</sup> (%)
				FDM	THFDM	HCPN	HHD	HXD	
1	Beta <sup>(d)</sup>	–	4	25	0	0	0	0	97
2	Beta <sup>(e)</sup>	–	10	N/A	0	0	0	0	90
3	Pd/Beta	2.8	80	1	3	3	56	8	77
4	Ru/Beta	2.7	41	2	7	2	44	7	84
5	Ni/Beta	8.7	21	19	0	24	19	0	93
6	Cu/Beta	9	24	13	4	0	25	0	88
7	Co/Beta	9.3	15	47	7	20	13	0	98
8	Pd/ZSM-5 <sup>(f)</sup>	2.9	74	1	1	1	41	14	74

<sup>(a)</sup> Metal chloride precursors. Reaction conditions: 0.23 g<sub>HMF</sub>, 45 ml H<sub>2</sub>O, 0.06 g<sub>cat</sub>, 110 °C, 20 bar H<sub>2</sub>, 600 rpm, 6 h.<sup>(b)</sup> Metal content based on ICP-OES measurements.<sup>(c)</sup> Carbon mass balance.<sup>(d)</sup> Si/Al = 12.5.<sup>(e)</sup> FDM as the substrate.<sup>(f)</sup> Si/Al = 11.5.

oligomerisation reactions which are favoured by the presence of acidic sites [24].

A preliminary control reaction with non-impregnated Beta zeolite (entry 1) showed negligible HMF conversion (4%) to FDM (1% yield), verifying that a reduced metal phase is essential for the conversion of HMF to the targeted diketone derivatives. An additional control experiment using the more reactive FDM intermediate as the substrate over Beta zeolite (entry 2) resulted in 10% FDM conversion with a concomitant colour change of the reaction mixture from pale to dark yellow. However, no products were detected by GC and carbon mass balance (C<sub>mb</sub>) was only 90%. The decrease in C<sub>mb</sub> suggests that the highly reactive unsaturated intermediates formed by the hydrolytic ring-opening of FDM, such as 1-hydroxyhex-3-ene-2,5-dione (HHED) [27,28], may lead to heavier ill-defined products, such as humins [38,39]. This undesired oligomerisation reaction always takes place in parallel with productive FDM conversion. It should be noted that decarboxylation of HHED to levulinic and formic acid [40] was not observed due to the highly reducing conditions employed.

Among the screened active metal phases, the Pd/Beta catalyst (entry 3) afforded the highest HMF conversion (80%) and selectivity to HHD (56%), whereas HXD was also detected as a minor product (8% selectivity). However, C<sub>mb</sub> was only 77%, consistent with the formation of undetectable oligomers. The Ru/Beta catalyst (entry 4) showed lower HMF conversion (41%) and HHD selectivity (44%). The non-noble metal based catalysts (*i.e.* Ni, Cu and Co, entries 5–7) showed even lower HMF conversion (15–24%) despite having considerably higher metal loadings. Moreover, selectivity to HHD was rather poor (13–25%), whereas HXD was not detected. It should be noted that the higher C<sub>mb</sub> observed for the Ru, Ni, Cu and Co supported catalysts (84–98%) is a direct consequence of the lower HMF conversion. The superior catalytic activity of Pd relative to other transition metals has also been demonstrated for the hydrogenation of HMF to THFDM in water, using Pd/C carbon [41] or Pd@MIL-101(Al)-NH<sub>2</sub> MOF [42].

The effect of the zeolitic support was also explored by using ZSM-5 (Si/Al = 11.5) instead of Beta (Si/Al = 12.5) and preparing Pd/ZSM-5 (entry 8). The latter also showed high HMF conversion (74%) and HHD selectivity (41%), albeit slightly lower than Pd/Beta. Notably, Pd/ZSM-5 afforded the highest selectivity to HXD (14%) which can be attributed to the higher concentration of Brønsted acid sites in ZSM-5 [43] and the different structural frameworks

(MFI in ZSM-5 vs. BEA in Beta) which affect the shape selectivity by either mass transfer or transition state effects [44,45]. Overall, both zeolite-supported Pd catalysts gave the highest HMF conversion and HHD selectivity but also showed the lowest C<sub>mb</sub> due to the formation of heavier undetectable oligomers [27,28].

In order to clarify the role of water in the reaction mechanism, an isotopic labelling experiment was performed using D<sub>2</sub>O as the solvent under the same reaction conditions (110 °C, 20 bar H<sub>2</sub>). GC-MS revealed the formation of [D<sub>3</sub>]-HHD and [D<sub>4</sub>]-HXD as the main products, as well as traces of [D<sub>4</sub>]-HCPN. FDM was also detected but it was not deuterated (Fig. S12). Specifically, higher *m/z* values were observed in the mass spectra of the products when D<sub>2</sub>O was employed as the solvent instead of H<sub>2</sub>O: *m/z* = 118 ([D<sub>4</sub>]-HCPN), 133 ([D<sub>3</sub>]-HHD) and 118 ([D<sub>4</sub>]-HXD) compared to *m/z* = 114 (HCPN), 130 (HHD) and 114 (HXD). This in turn suggests that two D<sub>2</sub>O molecules participate in the catalytic mechanism, specifically in the ring-opening of FDM *via* consecutive hydration-dehydration steps (Fig. 3), as originally proposed by Horvat *et al.* [40]. Importantly, none of the above compounds is formed in water-free reaction mixtures [7]. Therefore, H<sub>2</sub>O not only serves as an environmentally benign solvent but is also necessary for FDM ring-opening [46].

### 3.2. Influence of Pd particle size

The effect of the Pd particles size in the Beta zeolite-supported catalysts was also investigated. In addition to the catalyst prepared by IWI and PdCl<sub>2</sub> (Pd/Beta), two more catalysts were prepared by either (i) IWI and Pd(NO<sub>3</sub>)<sub>2</sub> as the precursor (Pd(n)/Beta) or (ii) DP-CP with urea and PdCl<sub>2</sub> (Pd(u)/Beta). Samples were then calcined and reduced as before. The different preparation methods led to different morphologies of the supported Pd nanoparticles (NPs), as deduced by TEM imaging (Fig. 4 and S13) and PXRD (Fig. S14).

The Pd/Beta catalyst (Fig. 4a) resulted in intermediate Pd NPs (average diameter of 5.2 ± 3.4 nm). Employment of Pd(NO<sub>3</sub>)<sub>2</sub> as the precursor (Fig. 4b) led to much larger Pd NPs with a significantly less uniform particle size distribution (average diameter of 16.2 ± 10.4 nm). The higher dispersion of Pd catalysts with PdCl<sub>2</sub> as the precursor has been ascribed to the formation of complex Pd<sub>x</sub>O<sub>y</sub>Cl<sub>z</sub> species on alumina/aluminosilicate surfaces [47,48]. The DP-CP method (Fig. 4c) resulted in the smallest Pd NPs and the

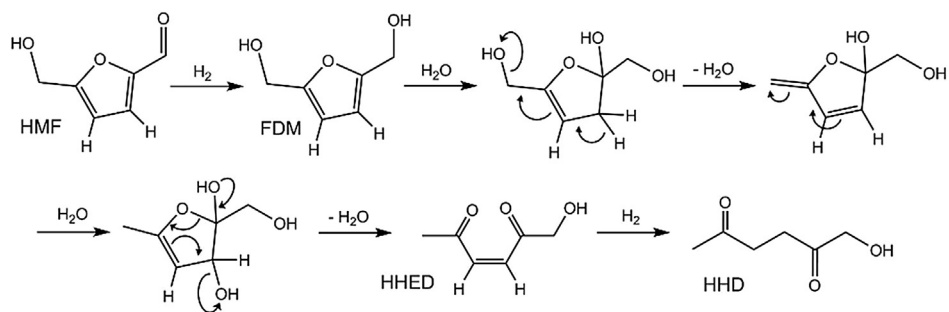


Fig. 3. Proposed mechanism for formation of HHD via double hydration/dehydration of the FDM intermediate [40], based on experiments carried out in  $D_2O$ .

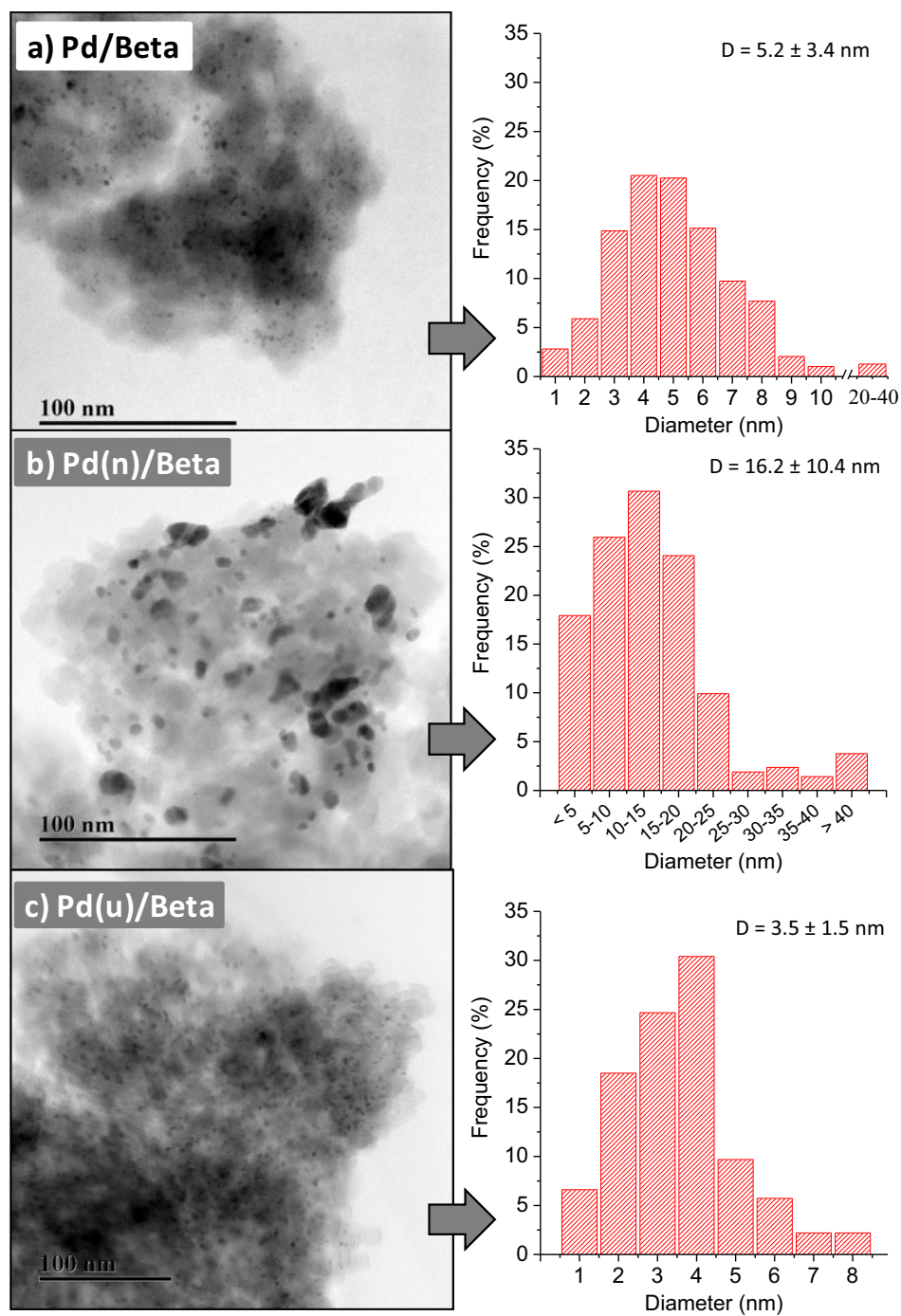


Fig. 4. TEM images and histograms of Pd particle size distribution (after counting >200 particles) of (a) Pd/Beta, (b) Pd(n)/Beta and (c) Pd(u)/Beta catalysts.

most uniform size distribution (average diameter of  $3.5 \pm 1.5$  nm). The smaller and more uniform particle size observed for Pd(u)/Beta can be associated with the slow and homogenous generation of hydroxide ions through the hydrolysis of urea at 95 °C which hinders the uneven precipitation of Pd<sup>II</sup> species due to a sudden, local increase of pH [49,50].

Table 2 shows the conversion of HMF and the obtained product distribution for the three Beta zeolite-supported Pd catalysts after 6 h under 20 bar of H<sub>2</sub> at 110 °C. All the catalysts have similar Pd contents varying between 2.6 and 2.8 wt% (based on ICP-OES). A direct correlation between higher HMF conversion and smaller Pd particle size was identified. Thus, the Pd(n)/Beta catalyst ( $d_M = 16.2 \pm 10.4$  nm) showed the lowest HMF conversion (56%). Moreover, the lower hydrogenation activity of Pd(n)/Beta resulted in the lowest selectivity to HHD (39%) due to a higher degree of oligomerisation of the unsaturated intermediates formed via FDM ring-opening (Fig. 3). On the other hand, the Pd(u)/Beta catalyst ( $d_M = 3.5 \pm 1.5$  nm) afforded almost complete HMF conversion (96%) and the highest selectivity to HHD (56%).

The N<sub>2</sub> adsorption-desorption isotherm of the Pd(u)/Beta catalyst was similar to the parent Beta zeolite (Fig. S15), presenting features of Type I isotherms. The resulting textural properties showed a slight decrease in specific surface area and pore volume after the incorporation of Pd ( $621 \text{ m}^2 \text{ g}^{-1}$  and  $0.297 \text{ cm}^3 \text{ g}^{-1}$  vs.  $574 \text{ m}^2 \text{ g}^{-1}$  and  $0.286 \text{ cm}^3 \text{ g}^{-1}$ ) due to partial blockage of the zeolite pores by Pd NPs, characteristic of a highly dispersed metal phase [51]. Thus, the enhanced hydrogenation activity with the decrease of Pd particle size can be attributed to the corresponding higher metal dispersion (higher metal active surface) [52] and to the higher uniformity in Pd particle size which favours the adsorption and hydrogenation of furanic compounds [41,42]. Additionally, well dispersed and uniform Pd NPs increase catalytic lifetime by hindering leaching and sintering of particles [53]. In this sense, SEM-EDX analysis of the Pd(u)/beta catalyst (Fig. S16) confirmed the absence of residual chlorine (from the PdCl<sub>2</sub> precursor) which is known to increase metal atom mobility and cause sintering.

The product distribution obtained over the Pd(u)/Beta catalyst (Table 2) revealed that at 96% HMF conversion no product exceeded 1% selectivity apart from the targeted diketone derivatives HHD and HXD. Notably, full conversion was achieved in 24 h and only two well-defined peaks corresponding to HXD and HHD were observed in the respective GC chromatogram of the product mixture (Fig. S17). However, C<sub>mb</sub> was found lower than 80% for all runs. Taken together, these observations suggest that an undetectable by GC fraction of products is produced via an acid-catalysed oligomerisation of unsaturated intermediates, formed via FDM ring-opening [24,27]. The formation of oligomers could be potentially suppressed by co-addition of organic solvents [54]. Alternatively, techniques such as biphasic reactive extraction, adsorbent-based separation or reactive distillation could be

applied to separate the oligomer fraction from the targeted compounds [55,56].

### 3.3. Time evolution of HMF conversion

The time evolution of HMF conversion, product distribution and C<sub>mb</sub> over the Pd(u)/Beta catalyst are depicted in Fig. 5. HMF was swiftly consumed, reaching 87% conversion in 120 min and 96% in 360 min. FDM was detected at early reaction times, with a maximum yield of 4% at 20 min but was fully consumed in 240 min. HHD and HXD yields rapidly increased during the first 120 min (47% and 7%, respectively) but did not significantly change afterwards, achieving final values of 54% (HHD) and 9% (HXD). Notably, exposing a mixture of HHD and HXD to a fresh batch of Pd(u)/Beta with or without H<sub>2</sub> (T = 110 °C, 3 h) showed no interconversion between HHD and HXD. A selectivity vs. conversion plot (Fig. S18) is consistent with HHD and HXD being formed via two separate pathways (Fig. 2). Previous works have shown that hydrogenolysis of FDM to DMF and hydrolysis of the latter can lead to HXD [21,25]. However, we did not detect any trace of DMF, indicating that HXD is formed through a currently unidentified mechanism.

The observed time profile supports the proposed reaction mechanism for the conversion of HMF into HHD (Fig. 3) which begins with the hydrogenation of the HMF carbonyl group to form FDM, followed by the hydrolytic furan ring-opening and hydrogenation to form HHD [10,17,20,28]. The intermediate nature of FDM was confirmed by a separate experiment using a lower amount of catalyst (40 mg instead of 60 mg); FDM yield reached a maximum of 23% before gradually decreasing as HHD was being formed (Fig. S19). The time evolution of the C<sub>mb</sub> showed a pronounced decrease within 120 min (from 100% to 73%) but remained practically constant afterwards (71% in 360 min). This is consistent with the formation of undetected heavier oligomers, catalysed by the zeolite acid sites.

### 3.4. Influence of support Si/Al ratio

Since the catalytic properties of the Pd(u)/Beta catalysts are directly related to the acidity of the zeolite framework, it was anticipated that the removal of Al atoms would affect catalyst activity and selectivity [57]. In order to understand the influence of the Si/Al ratio on the two competitive acid-catalysed reaction pathways, i.e. FDM ring-opening and oligomerisation of unsaturated intermediates, four Beta zeolite-supported Pd catalysts with different Si/Al ratio were prepared (Pd(u)/Beta-dAl<sub>x</sub>, x = 1–4) via dealumination (acid treatment) and subsequent Pd impregnation (DP-CP with PdCl<sub>2</sub>). The parent Beta zeolite (Si/Al = 12.5) was partially dealuminated by using gradually more concentrated HNO<sub>3</sub> aqueous solutions of 0.1, 0.5, 2 and 5 M which led to increasingly higher Si/Al atomic ratios in the range of 17.8–34.5 (Table 3).

**Table 2**

Product distribution from the conversion of HMF over Beta zeolite-supported Pd catalysts with different metal particle size.<sup>(a)</sup>

Catalyst	M <sup>(e)</sup> (wt%)	$d_M^{(f)}$ (nm)	Conv. (%)	Selectivity (%)					C <sub>mb</sub> (%)
				FDM	THFDM	HCPN	HHD	HXD	
Pd/Beta <sup>(b)</sup>	2.8	5.2	80	1	3	3	56	8	77
Pd(n)/Beta <sup>(c)</sup>	2.8	16.2	56	2	2	2	39	7	74
Pd(u)/Beta <sup>(d)</sup>	2.6	3.5	96	0	1	1	56	9	71

<sup>(a)</sup> Reaction conditions: 0.23 g<sub>HMF</sub>, 45 ml H<sub>2</sub>O, 0.06 g<sub>cat</sub>, 110 °C, 20 bar H<sub>2</sub>, 600 rpm, 6 h.

<sup>(b)</sup> IWI and PdCl<sub>2</sub>.

<sup>(c)</sup> IWI and Pd(NO<sub>3</sub>)<sub>2</sub>.

<sup>(d)</sup> DP-CP with urea and PdCl<sub>2</sub>.

<sup>(e)</sup> Metal content based on ICP-OES.

<sup>(f)</sup> Mean metal particle diameter based on TEM images.

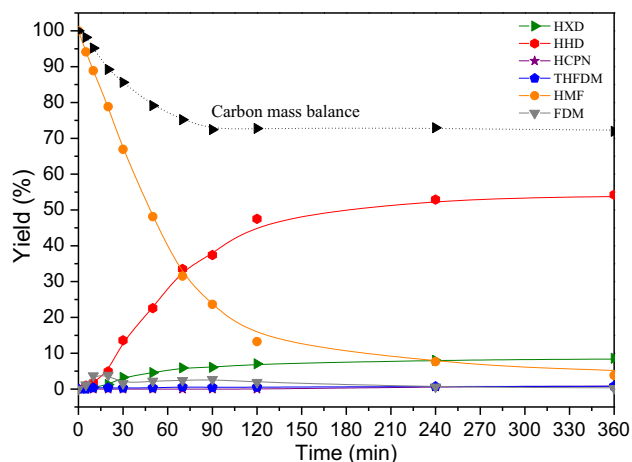


**Fig. 5.** Time evolution of HMF conversion to HHD over the Pd(u)/Beta catalysts. Reaction conditions: 0.23 g<sub>HMF</sub>, 45 ml H<sub>2</sub>O, 0.06 g<sub>cat</sub>, 110 °C, 20 bar H<sub>2</sub>, 600 rpm.

Crystallinity and microporosity of the zeolitic support were preserved after the dealumination treatment based on the respective PXRD patterns and N<sub>2</sub> isotherm profiles (Fig. SI10). Removal of Al resulted in a progressive decrease of acid sites according to NH<sub>3</sub>-TPD measurements (Fig. SI11 and Table SI2), due to removal of: (i) extra-framework aluminium, associated to Lewis acidity and (ii) tetrahedrally coordinated aluminium, associated to Brønsted acidity [58,59]. Important differences were observed in the catalytic performance of the Pd(u)/Beta-dAl<sub>x</sub> catalysts (Table 3). A non-negligible increase of C<sub>mb</sub> was observed over the dealuminated supports (from 71% for Pd(u)/Beta to 79–82% for Pd(u)/Beta-dAl<sub>x</sub>). However, a gradual decrease in HMF conversion and selectivity to HHD was also observed as the Si/Al ratio was increased due to the lower extent of the hydrolytic FDM ring-opening, catalysed by Brønsted acid sites.

### 3.5. Influence of temperature and H<sub>2</sub> pressure on HHD production

The effect of reaction temperature (80–155 °C) and H<sub>2</sub> pressure (5–60 bar) on the production of diketone derivatives from HMF over the Pd(u)/Beta catalyst was also investigated (Table 4). Comparison with the original run (entry 1) revealed that lowering the temperature below 110 °C resulted in lower HMF conversion (entries 2–3). Raising the temperature to 125 °C or 140 °C (entries 4–5) restored HMF conversion (≥95%). Notably, HCPN was also detected as a minor product (4–5% selectivity) as the temperature increased due to promotion of FDM ring-rearrangement, resulting in a slight improvement of C<sub>mb</sub> (from 71% at 110 °C to 78% at 140 °C). However, the combined selectivity of targeted HHD and HXD was practically not affected (65 ± 1%), although a marginal shift towards HXD was observed (56% HHD and 9% HXD at

110 °C vs. 53% HHD and 13% HXD at 140 °C). Further increasing the temperature to 155 °C (entry 6) led to a significant decrease of HHD selectivity, mainly due to oligomerisation (C<sub>mb</sub> = 65%).

Having established that T = 110 °C is the optimal temperature for the production of the targeted compounds, the effect of H<sub>2</sub> pressure was explored. Running the reaction under 40 bar of H<sub>2</sub> afforded again 96% HMF conversion, albeit with a slightly higher C<sub>mb</sub> (77%, entry 9). Increasing the H<sub>2</sub> pressure to 60 bar resulted in 98% HMF conversion with 66% HHD selectivity in 6 h and 100% conversion with 68% HHD selectivity in 24 h (entries 10–11). C<sub>mb</sub> increased to 82%, consistent with a faster hydrogenation rate of the unsaturated intermediates (vs. oligomerisation) to form HHD.

### 3.6. Stability and reusability studies

The stability of the Pd(u)/Beta catalyst was examined by testing the catalytic activity of the supernatant after physically separating the catalyst from the reaction mixture. HMF conversion did not increase any further (≈50% conversion at 110 °C and 20 bar H<sub>2</sub>) and product distribution did not change once the catalyst was filtered off after 40 min (Fig. SI12). Likewise, Pd concentration in the supernatant was less than 0.2 ppm (<0.5% of the total Pd content), according to ICP-OES. Both results verify that Pd does not leach into the solution phase and confirm the heterogeneous nature of the catalytic system.

The reusability of the Pd(u)/Beta catalyst was investigated by evaluating its catalytic activity upon consecutive runs (110 °C, 20 bar H<sub>2</sub>). The used catalyst was recovered after each run by filtration at room temperature, washed with deionized water and dried at 25 °C overnight. Fig. 6a depicts the TGA curves of the fresh and the used Pd(u)/Beta catalysts, showing a noticeable increase in the total weight loss for the used catalyst (28% vs. 7%). Furthermore, the elemental microanalysis of the used catalyst (Fig. 6a inset) revealed a significant carbon content (9.32% weight), consistent with deposition of organic compounds on the catalyst's surface during turnover. This result compensates to a certain extent (5–6%) for the lower C<sub>mb</sub> observed. The PXRD pattern of the used Pd(u)/Beta catalyst (Fig. 6b) showed the expected reflections of the Pd metallic phase, indicating that Pd remains reduced after turnover. However, TEM images of the used catalyst (Fig. 6c and SI13) revealed an increase in Pd particle size (d<sub>M</sub> = 7.6 ± 2.3 nm, Fig. 6d) compared to the fresh catalyst (d<sub>M</sub> = 3.5 ± 1.5 nm, Fig. 4c), indicative of aggregation and formation of larger Pd particles [60].

Recycling tests were conducted after recovering the Pd(u)/Beta catalyst (Fig. 7a). HMF conversion gradually decreased from 96% (1st run) to 10% (4th run) due to deposition of organic compounds and aggregation of Pd NPs (Fig. 6 and Fig. SI13). In order to restore the catalytic activity, the used Pd(u)/Beta catalyst (after 4 consecutive runs) was subjected to a regular regeneration treatment: calcination (air/500 °C/5h) and reduction (H<sub>2</sub>/200 °C/5h). Catalytic

**Table 3**  
Catalytic conversion of HMF to HHD and HXD over dealuminated Beta zeolite-supported Pd catalysts.<sup>(a)</sup>

Catalyst	Si/Al <sup>(b)</sup>	d <sub>M</sub> <sup>(c)</sup> (nm)	Conv. (%)	Selectivity (%)					C <sub>mb</sub> (%)
				FDM	THFDM	HCPN	HHD	HXD	
Pd(u)/Beta	12.5	11	96	0	1	1	56	9	71
Pd(u)/Beta-dAl1	17.8	11	70	1	1	1	53	11	79
Pd(u)/Beta-dAl2	20.6	12	64	2	2	1	47	16	81
Pd(u)/Beta-dAl3	27.0	14	52	2	2	0	42	12	80
Pd(u)/Beta-dAl4	34.5	15	49	4	2	2	39	12	82

<sup>(a)</sup> Reaction conditions: 0.23 g<sub>HMF</sub>, 45 ml H<sub>2</sub>O, 0.06 g<sub>cat</sub>, 110 °C, 20 bar H<sub>2</sub>, 600 rpm, 6 h.

<sup>(b)</sup> Based on SEM-EDX measurements.

<sup>(c)</sup> Mean metal particle diameter based on PXRD patterns and Scherrer equation.

**Table 4**  
Product distribution from the conversion of HMF over the Pd(u)/Beta catalyst.<sup>(a)</sup>

Entry	T (°C)	PH <sub>2</sub> (bar)	t (h)	Conv. (%)	Selectivity (%)					C <sub>mb</sub> (%)
					FDM	THFDM	HCPN	HHD	HXD	
1	110	20	6	96	0	1	1	56	9	71
2	80	20	6	67	3	1	0	39	3	68
3	95	20	6	88	1	1	0	57	6	71
4	125	20	6	96	0	1	4	54	10	75
5	140	20	6	95	0	1	5	53	13	78
6	155	20	6	99	1	2	7	37	14	65
7	110	5	6	69	0	0	1	48	9	73
8	110	10	6	90	0	1	1	59	8	75
9	110	40	6	96	1	1	2	61	7	77
10	110	60	6	98	1	1	1	66	7	82
11	110	60	24	100	0	2	2	68	8	82

<sup>(a)</sup> Reaction conditions: 0.23 g<sub>HMF</sub>, 45 ml H<sub>2</sub>O, 0.06 g<sub>cat</sub>, 600 rpm.

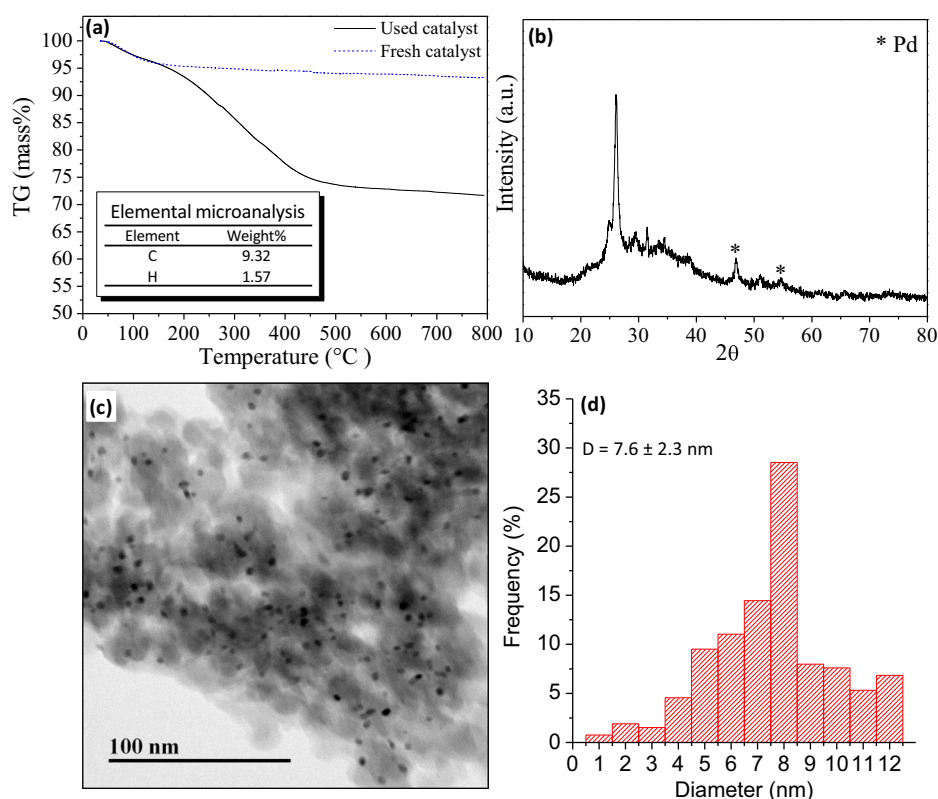


**Fig. 6.** (a) TGA curves (air, 100 cm<sup>3</sup> min<sup>-1</sup>) and C and H elemental microanalysis (inset), (b) PXRD pattern, (c) TEM image and (d) histogram of Pd particle size distribution (after counting >200 particles) of the used Pd(u)/Beta catalyst.

activity was partially restored (5th run), affording 90% HMF conversion to HHD (40% yield) and HXD (4% yield). A non-negligible amount of FDM (7% yield) and HCPN (12% yield) was also detected in the product mixture.

In order to investigate the observed change in selectivity, a separate set of experiments was conducted during which the catalyst was regenerated at the end of each run (Fig. 7b). HMF conversion gradually decreased from 96% (1st run) to 56% (3rd run) with a concomitant increase in FDM yield (6% in 3rd run), as also observed for the dealuminated samples (Table 3). Measurement of the <sup>27</sup>Al MAS NMR spectra of the fresh and the regenerated Pd(u)/Beta catalyst (Fig. S114) revealed a decrease in the fraction of tetrahedrally coordinated Al after turnover and regeneration. This in turn suggests a lower number of Brønsted acid sites [61] which promote

FDM ring-opening. Moreover, PXRD verified an increase in Pd particle size after regeneration (Fig. S115), consistent with a lower hydrogenation activity. Therefore, the observed differences in activity and selectivity during recycling can be ascribed to aggregation of Pd NPs and partial loss of Brønsted acidity [61–65].

#### 4. Conclusions

Diketone derivatives such as HHD and HXD were produced from HMF over a bifunctional Beta zeolite-supported Pd catalyst in water under relatively mild reaction conditions. The DP-CP method afforded the most active catalyst, compared to IW1, due to smaller and more uniformly dispersed Pd particles among the zeolitic support. Complete conversion of HMF was achieved at

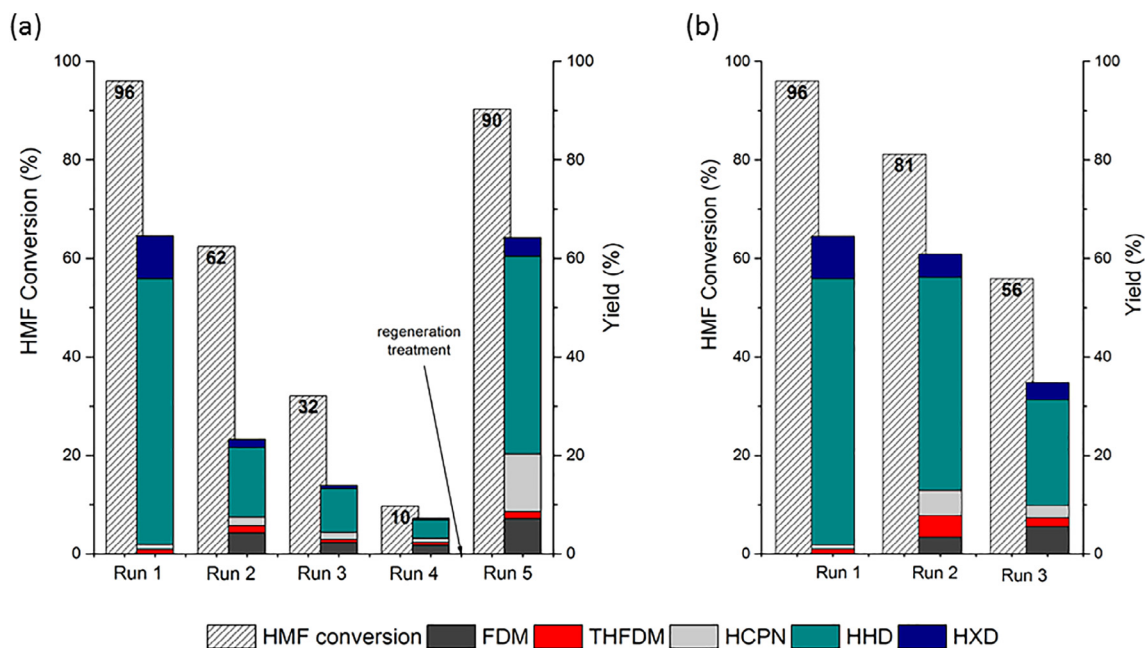


**Fig. 7.** HMF conversion (lined, left column) and product yield (right column) over the Pd(u)/Beta catalyst (6 h, 110 °C, 20 bar H<sub>2</sub>): (a) consecutive runs before (runs 1–4) and after catalyst regeneration (run 5); (b) consecutive runs after catalyst regeneration at the end of each run. C<sub>mb</sub> is less than 100% due to formation of heavier oligomers.

110 °C and 60 bar of H<sub>2</sub> with 68% selectivity to HHD. Leaching of Pd was not observed and catalytic activity could be partially restored after a simple regeneration step. Selectivity to HHD is mainly limited by the formation of heavier ill-defined oligomers. The key distinguishing feature of this study is the synergic effect of the zeolite acid sites and the highly active hydrogenating Pd metallic phase which promotes the hydrolytic ring-opening and subsequent hydrogenation of the FDM intermediate without necessitating co-addition of an acid or use of an organic solvent.

## Acknowledgements

This work was supported by the Engineering and Physical Sciences Research Council (EPSRC), UK (EP/K014749).

## Appendix A. Supplementary material

Supplementary data to this article can be found online at <https://doi.org/10.1016/j.jcat.2019.04.038>.

## References

- [1] Y.C. Lin, G.W. Huber, *Energy Environ. Sci.* 2 (2009) 68.
- [2] F. Cherubini, *Energy Convers. Manag.* 51 (2010) 1412.
- [3] T. Werpy, G. Petersen, A. Aden, J. Bozell, J. Holladay, J. White, A. Manheim, *Top Value Added Chemicals from Biomass: Results of Screening for Potential Candidates from Sugars and Synthesis Gas U.S. DoE Report*, NREL and Pacific Northwest National Laboratory, 2004.
- [4] J.J. Bozell, G.R. Petersen, *Green Chem.* 12 (2010) 539.
- [5] J.N. Chheda, Y. Román-Leshkov, J.A. Dumesic, *Green Chem.* 9 (2007) 342.
- [6] R.J. van Putten, J.C. van der Waal, E.D. De Jong, C.B. Rasrendra, H.J. Heeres, J.G. de Vries, *Chem. Rev.* 113 (2013) 1499.
- [7] S. Chen, R. Wojcieszak, F. Dumeignil, E. Marceau, S. Royer, *Chem. Rev.* 118 (2018) 11023.
- [8] R. Alamillo, M. Tucker, M. Chia, Y. Pagán-Torres, J.A. Dumesic, *Green Chem.* 14 (2012) 1413.
- [9] Y. Nakagawa, K. Takada, M. Tamura, K. Tomishige, *ACS Catal.* 4 (2014) 2718.
- [10] N. Perret, A. Grigoropoulos, M. Zanella, T.D. Manning, J.B. Claridge, M.J. Rosseinsky, *ChemSusChem* 9 (2016) 521.
- [11] Y. Román-Leshkov, C.J. Barrett, Z.Y. Liu, J.A. Dumesic, *Nature* 447 (2007) 982.
- [12] O. Casanova, S. Iborra, A. Corma, *ChemSusChem* 2 (2009) 1138.
- [13] S.E. Davis, B.N. Zope, R.J. Davis, *Green Chem.* 14 (2012) 143.
- [14] S. Yao, X. Wang, Y. Jiang, F. Wu, X. Chen, X. Mu, *ACS Sust. Chem. Eng.* 2 (2013) 173.
- [15] B. Xiao, M. Zheng, X. Li, J. Pang, R. Sun, H. Wang, X. Pang, A. Wang, S. Wang, T. Zhang, *Green Chem.* 18 (2016) 2175.
- [16] J. Ohyama, R. Kanao, Y. Ohira, A. Satsuma, *Green Chem.* 18 (2016) 676.
- [17] R. Ramos, A. Grigoropoulos, N. Perret, M. Zanella, A.P. Katsoulidis, T.D. Manning, J.B. Claridge, M.J. Rosseinsky, *Green Chem.* 19 (2017) 1701.
- [18] Z. Xu, P. Yan, H. Li, K. Liu, X. Liu, S. Jia, Z.C. Zhang, *ACS Catal.* 6 (2016) 3784.
- [19] B. Wozniak, Y. Li, S. Hünze, S. Tin, J.G. de Vries, *Eur. J. Org. Chem.* 17 (2018) 2009.
- [20] Z. Xu, P. Yan, W. Xu, X. Liu, Z. Xia, B. Chung, S. Jia, Z.C. Zhang, *ACS Catal.* 5 (2014) 788.
- [21] D. Ren, Z. Song, L. Li, Y. Liu, F. Jin, Z. Huo, *Green Chem.* 18 (2016) 3075.
- [22] J.J. Roylance, K.S. Choi, *Green Chem.* 18 (2016) 2956.
- [23] V. Schiavo, G. Descotes, J. Mentech, *Bull. Soc. Chim. Fr.* 128 (1991) 704.
- [24] Y. Nakagawa, M. Tamura, K. Tomishige, *ACS Catal.* 3 (2013) 2655.
- [25] J. Tuteja, H. Choudhary, S. Nishimura, K. Ebitani, *ChemSusChem* 7 (2014) 96.
- [26] G.C.A. Luijckx, N.P.M. Huck, F. van Rantwijk, L. Maat, H. van Bekkum, *Heterocycles* 77 (2009) 1037.
- [27] F. Liu, M. Audemar, K.D.O. Vigier, J.M. Clacens, F. De Campo, F. Jérôme, *ChemSusChem* 7 (2014) 2089.
- [28] F. Liu, M. Audemar, K. De Oliveira Vigier, J.-M. Clacens, F. De Campo, F. Jérôme, *Green Chem.* 16 (2014) 4110.
- [29] A. Corma, *J. Catal.* 216 (2013) 298.
- [30] B. Hernández, J. Iglesias, G. Morales, M. Paniagua, C. López-Aguado, J.L.G. Fierro, P. Wolf, I. Hermans, J.A. Melero, *Green Chem.* 18 (2016) 5777.
- [31] M.M. Antunes, S. Lima, P. Neves, A.L. Magalhães, E. Fazio, A. Fernandes, N. Fortunato, C.M. Silva, M. Ribeiro, M. Pillinger, A. Urakawa, A.A. Valente, *J. Catal.* 329 (2015) 522.
- [32] B.L. Wegenhart, L. Yang, S.C. Kwan, R. Harris, H.I. Kenttämaa, M.M. Abu-Omar, *ChemSusChem* 7 (2014) 2742.
- [33] L.A.M. Hermans, J.W. Geus, *Preparation of Catalysts II*, Elsevier, Amsterdam, 1979, p. 113.
- [34] M.E. Smith, E.R.H. van Eck, *Prog. Nucl. Magn. Reson. Spectrosc.* 34 (1999) 159.
- [35] J. Pérez-Pariente, J. Sanz, V. Fornés, A. Corma, *J. Catal.* 124 (1990) 217.
- [36] A. Abraham, S.-H. Lee, C.-H. Shin, S.B. Hong, R. Prins, J.A. van Bokhoven, *Phys. Chem. Chem. Phys.* 6 (2004) 3031.
- [37] J.B. Higgins, R.B. LaPierre, J.L. Schlenker, A.C. Rohrman, J.D. Wood, G.T. Kerr, W. J. Rohrbraugh, *Zeolites* 8 (1988) 446.
- [38] G. Tsilomelekis, M.J. Orella, Z. Lin, Z. Cheng, W. Zheng, V. Nikolakis, D.G. Vlachos, *Green Chem.* 18 (2016) 1983.
- [39] A. Gandini, M.N. Belgacem, *Prog. Polym. Sci.* 22 (1997) 1203.
- [40] J. Horvat, B. Klaić, B. Metelko, V. Sunjić, *Tetr. Lett.* 26 (1985) 2111.
- [41] H. Cai, C. Li, A. Wang, T. Zhang, *Catal. Today* 234 (2014) 59.
- [42] J. Chen, R. Liu, Y. Guo, L. Chen, H. Gao, *ACS Catal.* 5 (2014) 722.
- [43] F. Lónyi, J. Valyon, *J. Thermochim. Acta* 373 (2001) 53.
- [44] B. Smit, T.L. Maesen, *Chem. Rev.* 108 (2008) 4125.
- [45] J. Jae, G.A. Tompsett, A.J. Foster, K.D. Hammond, S.M. Auerbach, R.F. Lobo, G.W. Huber, *J. Catal.* 279 (2011) 257.
- [46] R. Ma, X.-P. Wu, T. Tong, Z.-J. Shao, Y. Wang, X. Liu, Q. Xia, X.-Q. Gong, *ACS Catal.* 7 (2017) 333.
- [47] M. Haneda, Y. Kintaichi, I. Nakamura, T. Fujitani, H. Hamada, *J. Catal.* 218 (2003) 405.

- [48] F.B. Noronha, M.A.S. Baldanza, M. Schmal, *J. Catal.* 188 (1999) 270.
- [49] W. Song, C. Zhao, J.A. Lercher, *Chem. Eur. J.* 19 (2013) 9833.
- [50] P. Burattin, M. Che, C. Louis, *J. Phys. Chem. B* 102 (1998) 2722.
- [51] R. Ramos, A. García, J.A. Botas, D.P. Serrano, *Ind. Eng. Chem. Res.* 55 (2016) 12723.
- [52] P. Mäki-Arvela, J. Hájek, T. Salmi, D.Y. Murzin, *Appl. Catal. A Gen.* 292 (2005) 1.
- [53] S.T. Gentry, S.F. Kendra, M.W. Bezpalko, *J. Phys. Chem. C* 115 (2011) 12736.
- [54] V.V. Ordomsky, J. Van der Schaaf, J.C. Schouten, T.A. Nijhuis, *J. Catal.* 287 (2012) 68.
- [55] H. Nguyen, R.F. DeJaco, N. Mittal, J.I. Siepmann, M. Tsapatsis, M.A. Snyder, W. Fan, B. Saha, D.G. Vlachos, *Annu. Rev. Chem. Biomol. Eng.* 8 (2017) 115.
- [56] P.S. Metkar, E.J. Till, D.R. Corbin, C.J. Pereira, K.W. Hutchenson, S.K. Sengupta, *Green Chem.* 17 (2015) 1453.
- [57] R. Srivastava, N. Iwasa, S.I. Fujita, M. Arai, *Catal. Lett.* 130 (2009) 655.
- [58] R. Baran, Y. Millot, T. Onfroy, J.M. Krafft, S. Dzwigaj, *Microp. Mesop. Mat.* 163 (2012) 122.
- [59] D.M. Roberge, H. Hausmann, W.F. Hölderich, *Phys. Chem. Chem. Phys.* 4 (2002) 3128.
- [60] Y.F. Han, D. Kumar, C. Sivadinarayana, D.W. Goodman, *J. Catal.* 224 (2004) 60.
- [61] Y. Xiong, W. Chen, J. Ma, Z. Chen, A. Zeng, *RSC Adv.* 5 (2015) 103695.
- [62] S. Vitolo, B. Bresci, M. Seggiani, M.G. Gallo, *Fuel* 80 (2001) 17.
- [63] A. Marcilla, M.I. Beltrán, R. Navarro, *J. Anal. Appl. Pyrol.* 74 (2005) 361.
- [64] B. Puértolas, A. Veses, M.S. Callén, S. Mitchell, T. García, J. Pérez-Ramírez, *ChemSusChem* 8 (2015) 3283.
- [65] S. Wan, C. Waters, A. Stevens, A. Gumidyala, R. Jentoft, L. Lobban, D. Resasco, R. Mallinson, S. Crossley, *ChemSusChem* 8 (2015) 552.